ACS APPLIED MATERIALS & INTERFACES

Letter

Cite This: ACS Appl. Mater. Interfaces 2018, 10, 6084−6089

www.acsami.org

Interface Engineering of Anchored Ultrathin TiO_2/MoS_2 Heterolayers for Highly-Efficient Electrochemical Hydrogen Production

Jia Liang,[†,‡] Caixing Wang,[†,‡] Peiyang Zhao,[†,‡] Yanrong Wang,[‡] Lianbo Ma,[‡] Guoyin Zhu,[‡] Yi Hu,[‡] Zhipeng Lu,[‡] Zhaoran Xu,[‡] Yue Ma,[‡] Tao Chen,[‡] Zuoxiu Tie,[‡] Jie Liu,*[,§] and Zhong Jin*[,‡]

[‡]Key Laboratory of Mesoscopic Chemistry of MOE and Collaborative Innovation Center of Chemistry for Life Sciences, School of Chemistry and Chemical Engineering, Nanjing University, Nanjing 210093, China

[§]Department of Chemistry, Duke University, Durham, North Carolina 27708, United States

Supporting Information

ABSTRACT: An efficient self-standing hydrogen evolution electrode was prepared by in situ growth of stacked ultrathin TiO_2/MoS_2 heterolayers on carbon paper ($CP@TiO_2@MoS_2$). Owing to the high overall conductivity, large electrochemical surface area and abundant active sites, this novel electrode exhibits an excellent performance for hydrogen evolution reaction (HER). Remarkably, the composite electrode shows a low Tafel slope of 41.7 mV/dec, and an ultrahigh cathodic current density of 550 mA/cm^2 at a very low overpotential of 0.25 V. This work presents a new universal strategy for the construction of effective, durable, scalable, and inexpensive electrodes that can be extended to other electrocatalytic systems.

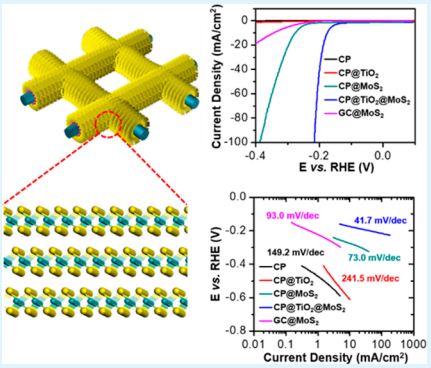

KEYWORDS: *molybdenum disulfide, titanium dioxide, self-standing, electrochemistry, hydrogen*

INTRODUCTION

Hydrogen generated from water splitting represents one of the most promising clean and renewable chemical energy carriers.[1,2] Among the existing routes for pure hydrogen production, hydrogen evolution reaction (HER), the electrocatalytic reduction of protons to molecular hydrogen, has attracted growing attentions.[3−5] Because of the low overpotential and fast kinetics, platinum (Pt) and other noble metals were widely investigated as the catalysts for HER.[6,7] However, to overcome the drawbacks of high cost and limited resources of noble metals, great efforts have been made to discover viable alternatives for HER catalysts. Over the past few decades, layered transition metal dichalcogenides (TMDCs) with the general formula of MX_2 (M = Co, Ni, Mo, W, etc.; X = S, Se, or Te),[8−12] have emerged as potential candidates to replace precious metals, owing to the highly active electrocatalytic performance and high stability.

Molybdenum disulfide (MoS_2), as a typical TMDC material with two-dimensional (2D) structure and semiconducting properties, has exhibited great promise for the applications in electrocatalysis.[13,14] Both theoretical and experimental results have revealed that the HER activity of MoS_2 is mainly resulted from the edge sites of S atoms, because the surface energy of edge planes is much higher than that of basal planes.[15] Compared to bulk MoS_2 crystals, ultrafine MoS_2 nanostructures with plenty of exposed edge sites can exhibit much higher electrocatalytic activity. In recent years, MoS_2 nanostructures and composites have been prepared and tested as HER catalysts, demonstrating reasonably good performances.[16−20] However, comparing with Pt or other noble materials, the overall conductivity, activity and stability of MoS_2 based electrocatalysts still need to be further improved. Especially, to improve the conductivity and electrocatalytic of electrode, it is very desirable to design novel free-standing composite electrode based on MoS_2 and three-dimensional (3D) conductive support materials, such as carbon nanomaterials. However, because of the intrinsic surface inertness and hydrophobic nature, it is difficult to firmly disperse and bind MoS_2 nanocrystals onto carbon frameworks. Therefore, the interfaces between MoS_2 and support materials should be well tuned, to ensure the strong interfacial binding, smooth charge transfer, and large effective surface area.

Herein, we report an effective approach to grow TiO_2/MoS_2 ultrathin heterolayers on commercial-available 3D-interconnected carbon paper (CP) with the help of a sandwiched intermediate layer of TiO_2. In this composite electrode, compact-packed MoS_2 nanolayer anchored on the surfaces of CP can expose large surface area and abundant active sites. The charge transfer between MoS_2 and CP is facilitated by the electron transfer layer of ultrathin TiO_2. Moreover, this self-standing electrode can be directly employed as the working electrode for HER without additional conductive additives and

Received: December 16, 2017
Accepted: February 8, 2018
Published: February 8, 2018

DOI: 10.1021/acsami.7b19009
ACS Appl. Mater. Interfaces 2018, 10, 6084−6089

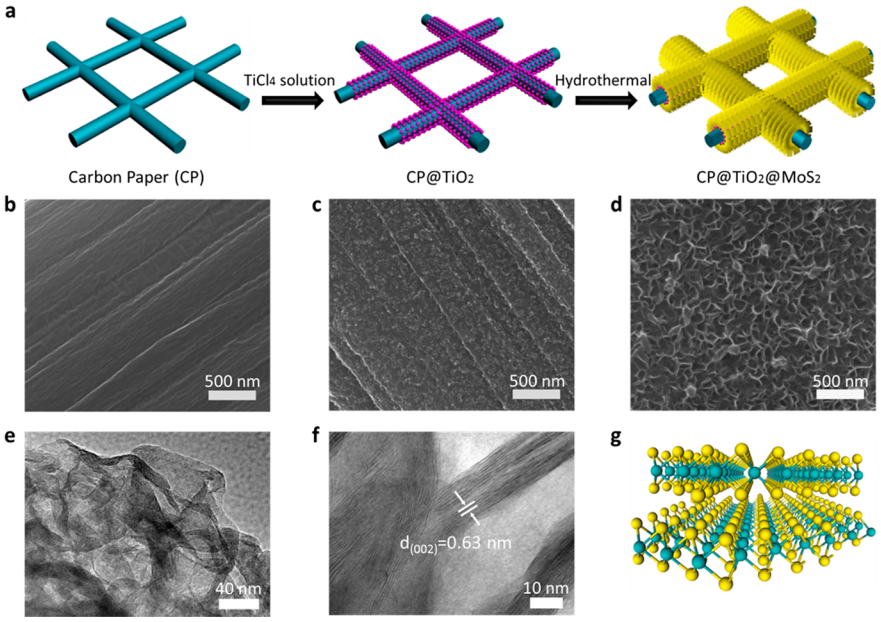

Figure 1. Schematic diagrams and structural characterizations of CP, CP@TiO_2 and CP@TiO_2@MoS_2 electrodes. (a) Synthesis process of CP@TiO_2@MoS_2 electrode. (b–d) SEM images of CP, CP@TiO_2 and CP@TiO_2@MoS_2 electrodes, respectively. (e, f) TEM and HRTEM images of ultrathin MoS_2 nanolayer anchored on CP@TiO_2@MoS_2 electrode. (g) Laminar crystalline structure of MoS_2 atomic layers.

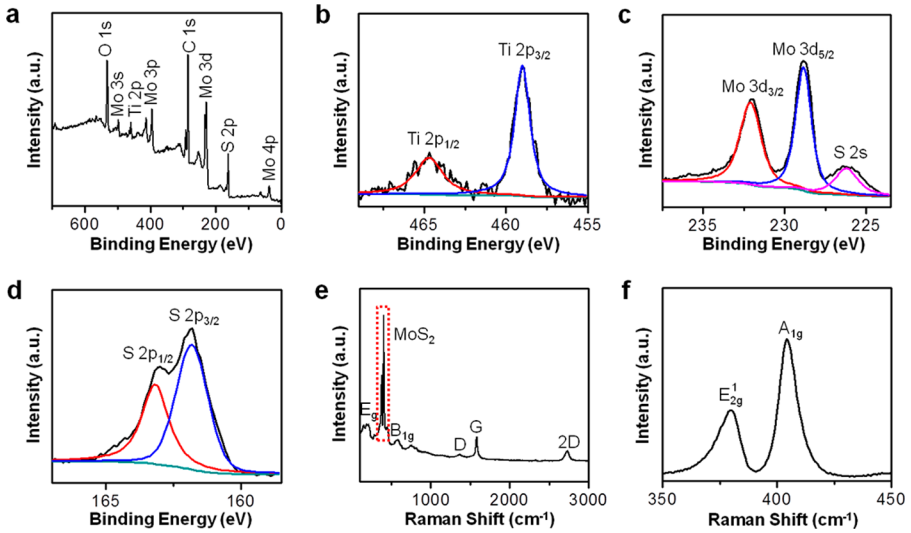

Figure 2. Characterizations of CP@TiO_2@MoS_2 electrodes. (a) Survey XPS spectrum and high-resolution XPS spectra at (b) Ti 2p, (c) Mo 3d ,and (d) S 2s regions of CP@TiO_2@MoS_2 electrode. (e) Raman spectrum of CP@TiO_2@MoS_2 electrode and (f) Raman peaks of E_{2g}^1 and A_{1g} vibrational modes of MoS_2 nanolayer magnified from e.

binders, thereby with high convenience. The CP@TiO_2@MoS_2 electrode exhibited excellent electrocatalytic activity with a small Tafel slope of 41.7 mV/dec. Especially, an ultrahigh cathodic current density of 550 mA/cm^2 was delivered at a low overpotential of 0.25 V, which is very remarkable compared to other MoS_2 based electrocatalysts in Table S1. Notably, the CP@TiO_2@MoS_2 electrode showed improved HER activity after 1000 CV sweeps, due to the decrease in charge-transfer resistance and the increase in effective surface area after electrochemical activation.

RESULTS AND DISCUSSION

Figure 1a shows the procedure for preparing CP@TiO_2@MoS_2 composite electrode. The CP substrate was first functionalized with a layer of ultrafine TiO_2 nanoparticles, termed as CP@TiO_2. Subsequently, a layer of densely packed and wrinkled MoS_2 nanosheet was in situ grown on the electrode. The surface morphologies of CP, CP@TiO_2, and CP@TiO_2@MoS_2 electrodes were further identified by scanning electronic microscopy (SEM, Figure 1b–d). The surface of pristine CP is clean and free of attached particles (Figure 1b). After treated with $TiCl_4$, a thin layer of TiO_2 nanoparticles were bonded onto CP substrate (Figure 1c). The average diameter of TiO_2 nanoparticles is ~10 nm, as shown in Figure S1. Figure 1d reveals the MoS_2 nanolayer uniformly fixed on the surface of CP@TiO_2@MoS_2 electrode through hydrothermal growth. Compared with bulk MoS_2 material, the MoS_2 nanolayer exhibits much larger active surface area and predominant edge sites, which are conducive to the electrocatalytic performances. Notably, the attachment of TiO_2 nanoparticles on the CP is

DOI: 10.1021/acsami.7b19009
ACS Appl. Mater. Interfaces 2018, 10, 6084–6089

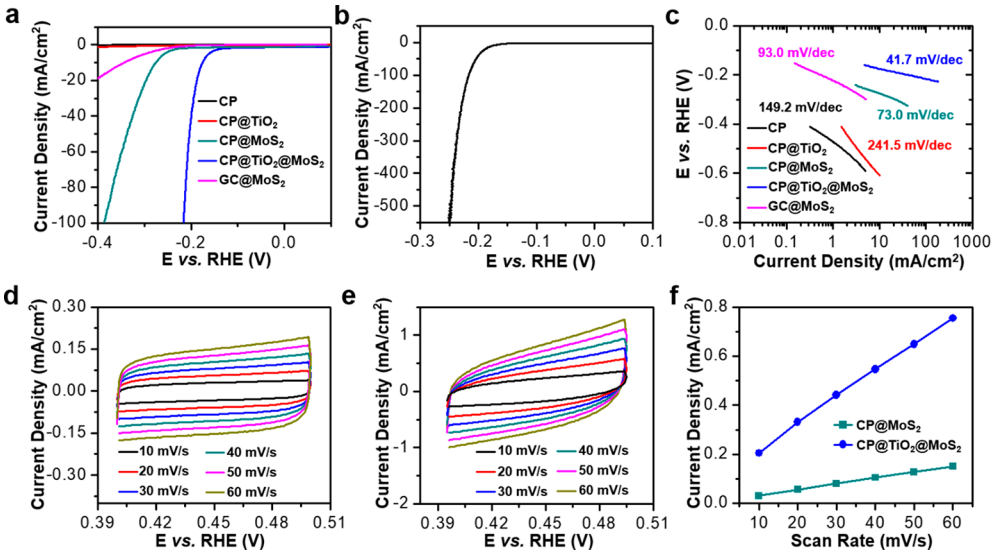

Figure 3. Electrocatalytic HER performances. (a) Polarization curves of CP, CP@TiO_2, CP@MoS_2, CP@TiO_2@MoS_2, and GC@MoS_2 electrodes at a scan rate of 5 mV/s, respectively. (b) Polarization curve of CP@TiO_2@MoS_2 electrode, showing a high cathodic current density of ~550 mA/cm^2 at an overpotential of 0.25 V. (c) Tafel plots of the electrodes calculated from a. CV curves of (d) CP@MoS_2 and (e) CP@TiO_2@MoS_2 electrodes collected in a selected potential range without Faradaic current at different scanning rates (10−60 mV/s), respectively. (f) Linear fitting of the capacitive current densities versus scanning rates of CP@MoS_2 and CP@TiO_2@MoS_2 electrodes calculated from d and e, respectively.

essential for the subsequent binding of MoS_2 nanolayer, because the TiO_2 nanolayer with high roughness can offer abundant high-energy nucleation sites for the nucleation and growth of MoS_2 nanosheet. For comparison, MoS_2 nanolayer was directly anchored onto the CP without the preceding step of TiO_2 nanoparticle attachment (labeled as CP@MoS_2), as shown in Figure S2, revealing that only a low density of MoS_2 nanoplatelets were randomly grown on CP.

Transmission electron microscopy (TEM) and high-resolution TEM (HRTEM) studies were performed to investigate the structure of CP@TiO_2@MoS_2 electrode. The TEM image of MoS_2 nanolayer (Figure 1e) reveals its ultrathin thickness and wrinkled, high-porosity structure. The cross-section HRTEM characterization of MoS_2 nanolayer (Figure 1f) shows the interlayer spacing of MoS_2 monolayers is 0.63 nm, which is in accordance with the (002) planes of hexagonal MoS_2 (Figure 1g).[21,22] Figure S3 displays a typical HRTEM image of the interface between TiO_2 and MoS_2, which clearly shows the surface of TiO_2 nanoparticles are fully covered by MoS_2 nanosheets and the contact between TiO_2 nanoparticles and MoS_2 nanosheets are very tight.

To identify the compositions of TiO_2/MoS_2 heterolayers, X-ray photoelectron spectroscopy (XPS) analysis was conducted (Figure 2a−d and Figure S4). The survey spectrum reveals the existence of C, Ti, O, Mo, and S elements (Figure 2a). The binding energies of Ti $2p_{1/2}$, Ti $2p_{3/2}$, and O 1s bands (Figure 2b and Figure S2b) are located at 464.7, 459, and 531.8 eV, respectively, indicating the formation of TiO_2 nanolayer.[23] The positions of Mo $3d_{5/2}$, Mo $3d_{3/2}$, S 2s, S $2p_{3/2}$, and S $2p_{1/2}$ bands (Figure 3c, d) are also determined and listed in Table S2, in accordance with the intrinsic features of MoS_2.[24]

Raman spectroscopic studies of CP@TiO_2@MoS_2 were also performed (Figure 2e, f). The D, G, and 2D bands of the CP substrate were revealed, while the peaks of E_g, B_{1g}, and E_g are assigned to anatase-phase TiO_2 (Figure 2e),[25−27] which is in agreement with the XPS results. Additionally, the two Raman peaks at 380.1 and 404.1 cm^{-1} are corresponding to the E_{2g}^1 and A_{1g} modes of MoS_2, respectively (Figure 2f). The E_{2g}^1 mode, also called the in-plane Mo−S phonon mode, is originated from the terrace-terminated MoS_2 layers; the A_{1g} mode, known as the out of plane Mo−S phonon mode, comes from the edge states of MoS_2.[28] As shown in Figure 2f, the integral intensity of the A_{1g} mode is twice than that of the E_{2g}^1 mode, indicating that the MoS_2 nanolayer is rich of edge sites.

The electrocatalytic HER activities of the electrodes were investigated in 0.5 M H_2SO_4 solution using a standard three-electrode setup. As another control sample, MoS_2 nanofilm was deposited onto glassy carbon electrode (labeled as GC@MoS_2, see the Experimental Methods section in the Supporting Information) and tested for comparison. Figure S5 shows the electrochemical impedance spectroscopy (EIS) analysis of these working electrodes, which reveals their excellent electrical conductivity. According to Figure S5, all the electrochemical data measured in this study were *iR* corrected. Figure 3a shows the polarization curves of CP, CP@TiO_2, CP@MoS_2, CP@TiO_2@MoS_2, and GC@MoS_2 electrodes, respectively. Clearly, the pristine CP and CP@TiO_2 electrodes display negligible HER activities, indicating that the high activity of CP@TiO_2@MoS_2 electrode comes from MoS_2 nanolayer, rather than CP substrate or TiO_2 layer. Moreover, the CP@TiO_2@MoS_2 electrode exhibits much higher HER activity than CP@MoS_2 and GC@MoS_2, suggesting that the rational designed MoS_2/TiO_2 heterolayers anchored on 3D interconnected CP is more favorable for HER. The overpotentials required for CP@MoS_2, GC@MoS_2, and CP@TiO_2@MoS_2 electrodes to reach a cathodic current density of 20 mA/cm^2 are 297, 344, and 188 mV, respectively. Because of the exceptional activity and conductivity, the CP@TiO_2@MoS_2 electrode delivers an ultrahigh current density of 550 mA/cm^2 at an overpotential of 250 mV (Figure 3b), as far as we know, which is record-breaking among the reported MoS_2-based catalysts (Table S1).

In HER experiments, the release rate of generated H_2 bubbles strongly affects the catalyst performance, especially under high cathodic current densities. Therefore, many previous studies employed a rotating disk electrode to dispel the H_2 bubbles away, which is impractical for large-scale

DOI: 10.1021/acsami.7b19009
ACS Appl. Mater. Interfaces 2018, 10, 6084−6089

deployment. In this study, the TiO_2/MoS_2 heterolayers grown on CP can vigorously release the evolved H_2 gas, as shown in Movie S1. Moreover, no obvious fluctuation can be found in the polarization curve of CP@TiO_2@MoS_2 electrode (Figure 3b), indicating the CP@TiO_2@MoS_2 electrode is very promising candidate for the use at large current densities.

The Tafel slopes of CP, CP@TiO_2, CP@MoS_2, CP@TiO_2@MoS_2 and GC@MoS_2 electrodes were plotted using the following equation: $\eta = b\log(j) + a$, where η, j, and b are the overpotential, current density and Tafel slope, respectively. Figure 3c shows the fitted Tafel slopes of CP, CP@TiO_2, CP@MoS_2, CP@TiO_2@MoS_2, and GC@MoS_2 electrodes are 149.2, 241.5, 73, 41.7, and 93 mV/dec, respectively. The CP and CP@TiO_2 electrodes display high Tafel slopes owing to the poor HER activity. The Tafel slope of CP@TiO_2@MoS_2 is much lower than those of CP@MoS_2, GC@MoS_2, indicating its superior activity and the predominate Volmer–Heyrovsky mechanism during HER process.

Effective surface area plays an important role for HER performance. The effective surface area of electrode is generally proportional to the electrochemical double layer capacitance. Therefore, the relative effective surface areas of CP@MoS_2 and CP@TiO_2@MoS_2 are compared by measuring the electrochemical double layer capacitances via cyclic voltammetry (CV) method (Figure 3d, e). A potential window between 0.4–0.5 V was selected for the test, because there is no Faradaic current in this range. The electrochemical double layer capacitances can be estimated from the slopes of the current density vs scan rate curves in Figure 3f. Clearly, the double layer capacitance of CP@TiO_2@MoS_2 is much larger than that of CP@MoS_2 within the same potential range, indicating the TiO_2 intermediate layer is very important for the growth of MoS_2 nanolayer with large effective surface area.

To investigate the effect of TiO_2 layer on the catalytic activity, we evaluated the turnover frequency (TOF) values of CP@MoS_2 and CP@TiO_2@MoS_2. The number of the active sites was determined by the electrochemical method.[29] Here, we propose a one-electron process for both reduction and oxidation, and then determined the upper limit of the active sites. Figure S6 shows the polarization curve normalized by the active sites and expressed in terms of TOF. Clearly, the CP@TiO_2@MoS_2 electrode exhibits higher catalytic activity than CP@MoS_2 electrode. Specifically, the overpotentials required for the CP@MoS_2 and CP@TiO_2@MoS_2 electrodes to reach a TOF value of 5 s^{-1} are 467 and 225 mV, respectively, which further indicates the TiO_2 intermediate layer is very important for the further decoration of MoS_2 nanolayer and the improvement of electrocatalytic performance.

To evaluate the activation and durability in acidic environment, we continuously cycled the CP@TiO_2@MoS_2 electrode for 1000 CV sweeps. The polarization curves of CP@TiO_2@MoS_2 electrode were measured before and after cycling (Figure 4a). The activated CP@TiO_2@MoS_2 electrode delivered cathodic current densities of 20 and 550 mA/cm^2 at the overpotentials of 177 and 232 mV, respectively, showing a further enhanced HER activity compared to that of the initial state. To obtain further insight into the electrode kinetic, EIS analysis of CP@TiO_2@MoS_2 working electrode was carried out before and after 1000 CV sweeps (Figure 4b). The Nyquist plots show dramatical decrease of charge transfer resistance after the CV cycling, confirming the activation effect. The change of effective surface area was also investigated by measuring CV curves of activated CP@TiO_2@MoS_2 electrode

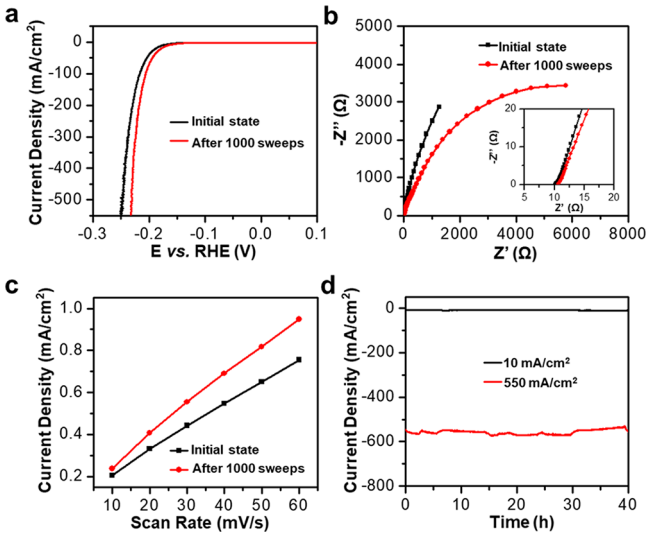

Figure 4. Stability test of CP@TiO_2@MoS_2 electrode. (a) Polarization curves, (b) Nyquist plots, and (c) fitted capacitive current densities vs scan rates of CP@TiO_2@MoS_2 electrode before and after 1000 CV sweeps, respectively. (d) Time-dependent cathodic current density of CP@TiO_2@MoS_2 electrode during HER process over 40 h at a fixed overpotential of 175 mV and 250 mV (after *iR* correction).

at different scan rates, as shown in Figure S7. Clearly, the electrochemical double layer capacitance of the CP@TiO_2@MoS_2 electrode after 1000 CV sweeps is higher than that of initial state (Figure 4c), suggesting the further enlarged effective surface area resulted from the electrolyte infiltration into the wrinkled and porous structure of MoS_2 nanolayer. In result, the decreased charge-transfer resistance and the enhanced effective surface area synergistically enhanced the electrocatalytic activity of CP@TiO_2@MoS_2 electrode.

To exclude the influence of Pt wire counter electrode, the HER activity of CP@TiO_2@MoS_2 electrode was also tested with graphite rod as counter electrode. The CP@TiO_2@MoS_2 electrode still shows an improved HER electrocatalytic activity after 1000 CV sweeps, as shown in Figure S8. The CP@TiO_2@MoS_2 electrode before and after 1000 CV sweeps delivered the cathodic current density of 20 mA/cm^2 at the overpotentials of 248 and 219 mV, respectively. This result confirms that the CP@TiO_2@MoS_2 electrode can exhibit enhanced HER performance after CV cycling, in spite of the different counter electrodes. It should be noted that the CP@TiO_2@MoS_2 electrode exhibits a slightly higher HER electrocatalytic activity with the aid of Pt wire counter electrode than graphite rod counter electrode, which can be ascribed to the higher activity of Pt wire.

The long-term stability for HER was also evaluated. It has been confirmed that the CP@TiO_2@MoS_2 electrode exhibits slightly enhanced HER electrocatalytic performance after continuous CV cycling. As shown in Figure 4d, the time-dependent cathodic current density of CP@TiO_2@MoS_2 at a fixed overpotential of 175 mV was measured, shows an observable enhancement after the long-time testing of 40 h. At a higher overpotential of 250 mV, the current density still remained relatively stable for over 40 h, showing the potential for practical long-term applications.

DOI: 10.1021/acsami.7b19009
ACS Appl. Mater. Interfaces 2018, 10, 6084–6089

CONCLUSION

In summary, we have rationally fabricated and anchored ultrathin TiO_2/MoS_2 heterolayers on conductive CP substrate as a self-standing electrode for high-efficiency electrocatalytic HER. The CP@TiO_2@MoS_2 electrode exhibited excellent electrocatalytic activity with small Tafel slope, remarkable cathodic current density at low overpotentials, and without obvious fluctuation in the polarization curve. Additionally, the electrode shows enhanced electrocatalytic activity after long-term CV sweeps, owing to the improved charge-transfer property and effective surface area. This work presents a novel scalable strategy for the fabrication of effective, durable, and cheap electrodes for electrocatalytic hydrogen production.

ASSOCIATED CONTENT

Supporting Information

The Supporting Information is available free of charge on the ACS Publications website at DOI: 10.1021/acsami.7b19009.

SEM images, TEM images, XPS curves, electrochemical performances, and tables (PDF)

Movie S1, showing that TiO_2/MoS_2 heterolayers grown on CP can vigorously release the evolved H_2 gas (AVI)

AUTHOR INFORMATION

Corresponding Authors

*E-mail: j.liu@duke.edu (J. L.).

*E-mail: zhongjin@nju.edu.cn (Z. J.).

ORCID

Jia Liang: 0000-0002-4352-1581

Jie Liu: 0000-0003-0451-6111

Zhong Jin: 0000-0001-8860-8579

Author Contributions

†J.L., C.W., and P.Z. contributed equally to this work.

Notes

The authors declare no competing financial interest.

ACKNOWLEDGMENTS

This work was supported by National Key Research and Development Program of China (2017YFA0208200, 2016YFB0700600), National Key Basic Research Program (2015CB659300), Projects of NSFC (21403105, 21573108), China Postdoctoral Science Foundation (2015M580412, 2015M581769), Natural Science Foundation of Jiangsu Province for Young Scholars (BK20150583, BK20160647), Fundamental Research Funds for the Central Universities (020514380107), and a project funded by the Priority Academic Program Development of Jiangsu Higher Education Institutions.

REFERENCES

(1) Subbaraman, R.; Tripkovic, D.; Strmcnik, D.; Chang, K.-C.; Uchimura, M.; Paulikas, A. P.; Stamenkovic, V.; Markovic, N. M. Enhancing Hydrogen Evolution Activity in Water Splitting by Tailoring Li^+-$Ni(OH)_2$-Pt Interfaces. *Science* **2011**, *334*, 1256.

(2) Caban-Acevedo, M.; Stone, M. L.; Schmidt, J. R.; Thomas, J. G.; Ding, Q.; Chang, H.-C.; Tsai, M.-L.; He, J.-H.; Jin, S. Efficient Hydrogen Evolution Catalysis using Ternary Pyrite-type Cobalt Phosphosulphide. *Nat. Mater.* **2015**, *14*, 1245.

(3) Nagasaka, M.; Kondoh, H.; Amemiya, K.; Ohta, T.; Iwasawa, Y. Proton Transfer in a Two-Dimensional Hydrogen-Bonding Network: Water and Hydroxyl on a Pt(111) Surface. *Phys. Rev. Lett.* **2008**, *100*, 106101.

(4) Gao, M.-R.; Liang, J.-X.; Zheng, Y.-R.; Xu, Y.-F.; Jiang, J.; Gao, Q.; Li, J.; Yu, S.-H. An Efficient Molybdenum Disulfide/Cobalt Diselenide Hybrid Catalyst for Electrochemical Hydrogen Generation. *Nat. Commun.* **2015**, *6*, 5982.

(5) Fei, H.; Dong, J.; Arellano-Jimenez, M. J.; Ye, G.; Kim, N. D.; Samuel, E. L. G.; Peng, Z.; Zhu, Z.; Qin, F.; Bao, J.; Yacaman, M. J.; Ajayan, P. M.; Chen, D.; Tour, J. M. Atomic Cobalt on Nitrogen-doped Graphene for Hydrogen Generation. *Nat. Commun.* **2015**, *6*, 8668.

(6) Kemppainen, E.; Bodin, A.; Sebok, B.; Pedersen, T.; Seger, B.; Mei, B.; Bae, D.; Vesborg, P. C. K.; Halme, J.; Hansen, O.; Lund, P. D.; Chorkendorff, I. Scalability and Feasibility of Photoelectrochemical H_2 Evolution: the Ultimate Limit of Pt Nanoparticle as an HER Catalyst. *Energy Environ. Sci.* **2015**, *8*, 2991.

(7) Zhou, W.; Jia, J.; Lu, J.; Yang, L.; Hou, D.; Li, G.; Chen, S. Recent Developments of Carbon-based Electrocatalysts for Hydrogen Evolution Reaction. *Nano Energy* **2016**, *28*, 29.

(8) Batmunkh, M.; Shrestha, A.; Gao, G.; Yu, L.-P; Zhao, J.; Biggs, M.-J.; Shearer, C.-J.; Shapter, J.-G. Sulfur-Doped Graphene with Iron Pyrite (FeS_2) as an Efficient and Stable Electrocatalyst for the Iodine Reduction Reaction in Dye-Sensitized Solar Cells. *Solar RRL* **2017**, *1*, 1700011.

(9) Kong, D.; Wang, H.; Lu, Z.; Cui, Y. $CoSe_2$ Nanoparticles Grown on Carbon Fiber Paper: An Efficient and Stable Electrocatalyst for Hydrogen Evolution Reaction. *J. Am. Chem. Soc.* **2014**, *136*, 4897.

(10) Kong, D.; Cha, J. J.; Wang, H.; Lee, H. R.; Cui, Y. First-row Transition Metal Dichalcogenide Catalysts for Hydrogen Evolution Reaction. *Energy Environ. Sci.* **2013**, *6*, 3553.

(11) Liang, J.; Yang, Y.; Zhang, J.; Wu, J.; Dong, P.; Yuan, J.; Zhang, G.; Lou, J. Metal Diselenide Nanoparticles as Highly Active and Stable Electrocatalysts for the Hydrogen Evolution Reaction. *Nanoscale* **2015**, *7*, 14813.

(12) Lin, J.; Peng, Z.; Wang, G.; Zakhidov, D.; Larios, E.; Yacaman, M. J.; Tour, J. M. Enhanced Electrocatalysis for Hydrogen Evolution Reactions from WS_2 Nanoribbons. *Adv. Energy Mater.* **2014**, *4*, 1301875.

(13) Huang, X.; Zeng, Z.; Bao, S.; Wang, M.; Qi, X.; Fan, Z.; Zhang, H. Solution-phase Epitaxial Growth of Noble Metal Nanostructures on Dispersible Single-layer Molybdenum Disulfide Nanosheets. *Nat. Commun.* **2013**, *4*, 1444.

(14) Li, Y.; Wang, H.; Xie, L.; Liang, Y.; Hong, G.; Dai, H. MoS_2 Nanoparticles Grown on Graphene: An Advanced Catalyst for the Hydrogen Evolution Reaction. *J. Am. Chem. Soc.* **2011**, *133*, 7296.

(15) Jaramillo, T. F.; Jorgensen, K. P.; Bonde, J.; Nielsen, J. H.; Horch, S.; Chorkendorff, I. Identification of Active Edge Sites for Electrochemical H_2 Evolution from MoS_2 Nanocatalysts. *Science* **2007**, *317*, 100.

(16) Zhu, H.; Zhang, J.; Yanzhang, R.; Du, M.; Wang, Q.; Gao, G.; Wu, J.; Wu, G.; Zhang, M.; Liu, B.; Yao, J.; Zhang, X. When Cubic Cobalt Sulfide Meets Layered Molybdenum Disulfide: A Core-Shell System Toward Synergetic Electrocatalytic Water Splitting. *Adv. Mater.* **2015**, *27*, 4752.

(17) Zhou, W.; Yin, Z.; Du, Y.; Huang, X.; Zeng, Z.; Fan, Z.; Liu, H.; Wang, J.; Zhang, H. Synthesis of Few-layer MoS_2 Nanosheet-coated TiO_2 Nanobelt Heterostructures for Enhanced Photocatalytic Activities. *Small* **2013**, *9*, 140.

(18) Yan, Y.; Xia, B.; Li, N.; Xu, Z.; Fisher, A.; Wang, X. Vertically oriented MoS_2 and WS_2 Nanosheets Directly Grown on Carbon Cloth as Efficient and Stable 3-Dimensional Hydrogen-Evolving Cathodes. *J. Mater. Chem. A* **2015**, *3*, 131.

(19) Yan, Y.; Ge, X.; Liu, Z.; Wang, J.; Lee, J.; Wang, X. Facile Synthesis of Low Crystalline MoS_2 Nanosheet-coated CNTs for Enhanced Hydrogen Evolution Reaction. *Nanoscale* **2013**, *5*, 7768.

(20) Zhao, L.; Jia, J.; Yang, Z.; Yu, J.; Wang, A.; Sang, Y.; Zhou, W.; Liu, H. One-step Synthesis of CdS Nanoparticles/MoS_2 Nanosheets Heterostructure on Porous Molybdenum Sheet for Enhanced Photocatalytic H_2 Evolution. *Appl. Catal., B* **2017**, *210*, 290.

(21) Najmaei, S.; Liu, Z.; Zhou, W.; Zou, X.; Shi, G.; Lei, S.; Yakobson, B.; Idrobo, J.; Ajayan, P.; Lou, J. Vapour Phase Growth and

Grain Boundary Structure of Molybdenum Disulphide Atomic Layers. *Nat. Mater.* **2013**, *12*, 754.
(22) Xie, J.; Zhang, J.; Li, S.; Grote, F.; Zhang, X.; Zhang, H.; Wang, R.; Lei, Y.; Pan, B.; Xie, Y. Controllable Disorder Engineering in Oxygen-incorporated MoS2 Ultrathin Nanosheets for Efficient Hydrogen Evolution. *J. Am. Chem. Soc.* **2013**, *135*, 17881.
(23) Chen, X. B.; Burda, C. Photoelectron Spectroscopic Investigation of Nitrogen-Doped Titania Nanoparticles. *J. Phys. Chem. B* **2004**, *108*, 15446.
(24) Weber, T.; Muijsers, J. C.; vanWolput, H. J. M. C.; Verhagen, C. P. J.; Niemantsverdriet, J. W. Basic Reaction Steps in the Sulfidation of Crystalline MoO_3 to MoS_2, As Studied by X-ray Photoelectron and Infrared Emission Spectroscopy. *J. Phys. Chem.* **1996**, *100*, 14144.
(25) Ferrari, A. C.; Meyer, J. C.; Scardaci, V.; Casiraghi, C.; Lazzeri, M.; Mauri, F.; Piscanec, S.; Jiang, D.; Novoselov, K. S.; Roth, S.; Geim, A. K. Raman Spectrum of Graphene and Graphene Layers. *Phys. Rev. Lett.* **2006**, *97*, 187401.
(26) Ohsaka, T.; Izumi, F.; Fujiki, Y. Raman Spectrum of Anatase, TiO_2. *J. Raman Spectrosc.* **1978**, *7* (6), 321.
(27) Li, H.; Zhang, Q.; Yap, C. C. R.; Tay, B. K.; Edwin, T. H. T.; Olivier, A.; Baillargeat, D. From Bulk to Monolayer MoS_2: Evolution of Raman Scattering. *Adv. Funct. Mater.* **2012**, *22* (7), 1385.
(28) Wang, H.; Lu, Z.; Xu, S.; Kong, D.; Cha, J.; Zheng, G.; Hsu, P.; Yan, K.; Bradshaw, D.; Prinz, F.; Cui, Y. Electrochemical Tuning of Vertically Aligned MoS_2 Nanofilms and its Application in Improving Hydrogen Evolution Reaction. *Proc. Natl. Acad. Sci. U. S. A.* **2013**, *110*, 19701.
(29) Ma, L.; Hu, Y.; Zhu, G.; Chen, R.; Chen, T.; Lu, H.; Wang, Y.; Liang, J.; Liu, H.; Yan, C.; Tie, Z.; Jin, Z.; Liu, J. In Situ Thermal Synthesis of Inlaid Ultrathin MoS_2/Graphene Nanosheets as Electrocatalysts for the Hydrogen Evolution Reaction. *Chem. Mater.* **2016**, *28*, 5733.

DOI: 10.1021/acsami.7b19009
ACS Appl. Mater. Interfaces 2018, 10, 6084−6089